

# Metal-Organic Framework Thin Films Grown on Functionalized Graphene as Solid-State Ion-Gated FETs

Abhinav Chandresh, Christof Wöll, and Lars Heinke\*

The unique properties of 2D-materials like graphene are exploited in various electronic devices. In sensor applications, graphene shows a very high sensitivity, but only a low specificity. This shortcoming can be mastered by using heterostructures, where graphene is combined with materials exhibiting high analyte selectivities. Herein, this study demonstrates the precise deposition of nanoporous metal-organic frameworks (MOFs) on graphene, yielding bilayers with excellent specificity while the sensitivity remains large. The key for the successful layer-by-layer deposition of the MOF films (SURMOFs) is the use of planar polyaromatic anchors. Then, the MOF pores are loaded with ionic liquid (IL). For functioning sensor devices, the IL@MOF films are grown on graphene field-effect transistors (GFETs). Adding a top-gate electrode yields an ion-gated GFET. Analysis of the transistor characteristics reveals a clear Dirac point at low gate voltages, good on-off ratios, and decent charge mobilities and densities in the graphene channel. The GFET-sensor reveals a strong and selective response. Compared to other ion-gated-FET devices, the IL@MOF material is relatively hard, allowing the manufacturing of ultrathin devices. The new MOF-anchoring strategy offers a novel approach generally applicable for the functionalization of 2D-materials, where MOF/2D-material hetero-bilayers carry a huge potential for a wide variety of applications.

for sensing applications. The first experimentally realized 2D material was graphene. Because of the strong interest in these materials, various methods have been developed to grow these ultrathin carbon films with a honeycomb crystal lattice structure<sup>[5]</sup> on industrially large scales.<sup>[6,7]</sup> Graphene possesses extraordinary physico-chemical and opto-electronic properties, such as a high charge carrier mobility, a high electrical conductivity with optical transparency, a large surface-to-volume ratio, and a huge mechanical strength.<sup>[8]</sup> Based on these unique properties, graphene alone or combined with other materials has been used for fabricating devices,<sup>[8,9]</sup> able to detect or measure biomolecules,<sup>[10]</sup> temperature,<sup>[11]</sup> pressure,<sup>[12]</sup> light,<sup>[13]</sup> and gases.<sup>[14]</sup>

Sensors based on electronic properties generally show fast and reproducible responses and allow for small device sizes.<sup>[15]</sup> In this context, graphene-based field-effect transistors (GFETs) have drawn particular interest.<sup>[16]</sup> A typical GFET includes three electrodes (drain, source, and gate), an insulating dielectric layer, and graphene (mono- or multilayers) as the

semiconducting channel material. In a GFET-based sensor, the change of the electronic properties of the channel material to external stimuli, i.e., the adsorption of chemical compounds, affects the conduction properties of the FET, which can be readily detected.

Typically, the insulator material between the gate and the channel is silicon dioxide (SiO<sub>2</sub>), with a thickness from 90 to 300 nm. One key feature of conventional GFETs is the presence of a conductance minimum with a charge neutrality point at a certain gate voltage, referred to as Dirac point.<sup>[17]</sup> For a typical GFET, starting from a negative gate voltage (or a low gate voltage) increasing the gate voltage, a decrease in (drain-source) current is observed until the Dirac point (with a minimum of conductivity) is reached. Further increasing the gate voltage results in an increase of the drain-source current.<sup>[17]</sup> The Dirac point and the charge carrier density of graphene are very sensitive to the local electric field, thus, the gate-voltage-dependence of it in GFETs is often exploited as a signal in sensors.

While GFET-based sensors possess the advantage of very high sensitivities, their response is rather unspecific, and it is difficult to differentiate between different analytes.<sup>[18]</sup> To overcome

## 1. Introduction

2D materials are atomically thin crystalline materials firmly held together by strong covalent bonds. Often they form stacks, with the individual sheets interacting via weak van-der-Waals forces.<sup>[1,2]</sup> Among the fascinating properties of these materials is their sensitivity to external stimuli,<sup>[3,4]</sup> thus offering their use

A. Chandresh, C. Wöll, L. Heinke  
Karlsruhe Institute of Technology (KIT)  
Institute of Functional Interfaces (IFG)  
Hermann-von-Helmholtz-Platz 1, 76344 Eggenstein-Leopoldshafen,  
Germany  
E-mail: lars.heinke@kit.edu

 The ORCID identification number(s) for the author(s) of this article can be found under <https://doi.org/10.1002/adfm.202211880>

© 2023 The Authors. Advanced Functional Materials published by Wiley-VCH GmbH. This is an open access article under the terms of the Creative Commons Attribution-NonCommercial License, which permits use, distribution and reproduction in any medium, provided the original work is properly cited and is not used for commercial purposes.

DOI: 10.1002/adfm.202211880

this limitation, graphene is combined with other functional materials to achieve an analyte-specific response.<sup>[19]</sup> A promising path to increase the selectivity of GFET-sensors was recently realized by growing metal-organic framework (MOF) films on graphene.<sup>[20]</sup> MOFs are nanoporous, crystalline materials composed of metal nodes connected by di- or higher-topic organic linkers.<sup>[21]</sup> MOFs possess well-defined adsorption sites, resulting in analyte-specific adsorption in sensor applications.<sup>[22–24]</sup> MOF materials can also be grown as thin films directly on a solid substrate, e.g., by employing layer-by-layer methods, resulting in surface-mounted MOFs, referred to as SURMOFs.<sup>[25,26]</sup> Since the poor adhesion properties of graphene prohibit the direct growth of the MOF film, the graphene surface was functionalized by deposition of an adhesion layer ( $\approx 5$  nm) of aluminum oxide to support the SURMOF growth in this previous work.<sup>[20]</sup> However, the presence of the adhesion layer represents a barrier that makes the direct contact of guests (e.g., ionic liquids) with the graphene impossible. To date, the direct anchoring of MOF films on graphene without the presence of an adhesion layer (or without suppressing the electronic graphene properties) has not been accomplished.

Generally, the gate voltages required for operating GFETs are fairly large, on the order of several tens of volts, since the  $\text{SiO}_2$ -layer used in the conventional designs to insulate the gate electrode from the graphene channel has a thickness in the order of 100 nm. This restricts the use of GFET-based sensors in low-power sensing applications. An approach to reduce the voltages is to use materials with a high dielectric constant. Indeed, a substantial lowering of the operational voltages in GFET was realized by using electrolytes.<sup>[27,28]</sup> There, the electric field generated by applying an external voltage is amplified by the formation of an electric double layer at the graphene-electrolyte interface.<sup>[29]</sup> Particularly attractive electrolytes in this context are ionic liquids (ILs), organic salts having a low melting point and a negligible small vapor pressure.<sup>[30]</sup> While ILs have been successfully used as gating material for GFET sensors,<sup>[31,32]</sup> the fluid nature of ILs severely complicates their integration into devices. In order to turn these liquids into solids, ILs have been blended with various materials, like polymers, resulting in the formation of ion-gels.<sup>[33,34]</sup> However, the low mechanical strength has so far prohibited the fabrication of robust small sensor devices.

Apart from sensing applications, ion-gated-transistors are fundamental for iontronics, which is an interdisciplinary field aiming for ion-based information transfer, mimicking the operation principle of electronic devices.<sup>[35,36]</sup> ILs have been successfully used in numerous applications in iontronic devices, like in enzymatic sensing and neuromorphic synaptic transistors.<sup>[37,38]</sup> In iontronics (like in sensor technologies), ILs are often combined with polymers making ion-gels. An alternative approach can be the embedment of the ILs in solid nanoporous materials, like MOFs, resulting in solid materials hosting mobile ions.<sup>[39]</sup> The structure and properties of the IL@MOF materials can be tuned to a wide extent and the motion of the ions in such solid nanoporous confinement under the influence of an electric field may deviate significantly from the dynamics of the unconfined (bulk) IL.<sup>[40–42]</sup>

One main challenge with regard to the fabrication of MOF-based GFETs is the functionalization of the graphene to enable the MOF growth. While first depositing aluminum oxide allows

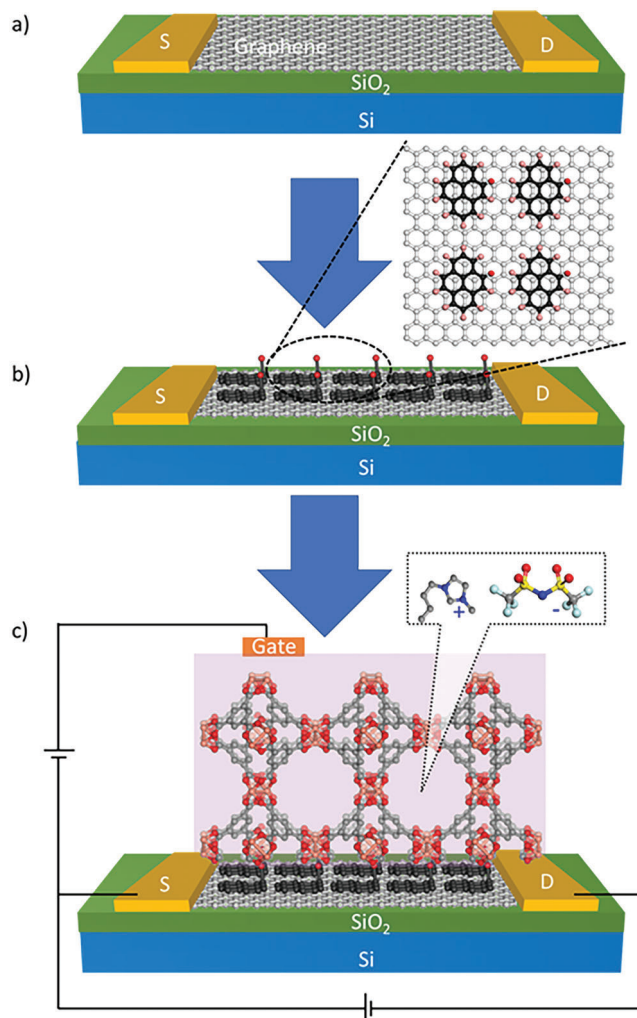


**Figure 1.** Fabrication of IL@SURMOF/GFET device. a) Sketch of the pristine GFET device. b) Functionalization of graphene with Pyr- $\text{CH}_2\text{OH}$ . c) Sketch of the device with electrical connections. The pores of the SURMOF (of type HKUST-1) are filled with IL (of type  $[\text{BMIM}]^+[\text{TFSI}]^-$ ) and an indium metal patch is deposited as a top gate electrode on top of the IL@SURMOF/GFET.

the growth of crystalline and oriented SURMOF films,<sup>[20]</sup> the interface between the MOF and the substrate as well as between the graphene and aluminum oxide are only poorly defined. In addition, in the context of ion-gated GFETs this approach cannot be used, since the thickness of the  $\text{Al}_2\text{O}_3$  layer ( $\approx 5$  nm) prohibits the required close proximity of the IL to the graphene layer.

The new strategy presented here is to employ anchors containing planar, polycyclic aromatic hydrocarbons like pyrene. Such planar compounds interact quite strongly with graphene and form stable, well-defined monolayers on the graphene surface.<sup>[43]</sup> Of course, in order to provide a docking site for the MOF constituents, these planar compounds need to be functionalized, e.g., by attaching OH groups. Indeed, regular, dense monolayers of 1-pyrenemethanol (Pyr- $\text{CH}_2\text{OH}$ ) with strong  $\pi$ - $\pi$  interaction between the graphene substrate and the pyrene adsorbates have been reported.<sup>[44]</sup> **Figure 1b,c** shows that the spacing of

the methoxy-groups in such a 2D layer fit well with the structure of the HKUST-1 MOF. After deposition, the pores of the SURMOFs were loaded with an ionic liquid. We chose HKUST-1,<sup>[45]</sup> a popular MOF for which the LBL process has been carefully optimized with respect to getting flat, highly oriented, and low-defect density crystalline thin films.<sup>[46]</sup> HKUST-1 has a face centered cubic structure with pores of  $\approx 0.9$  nm in diameter. HKUST-1 is a non-conducting MOF with a conductivity in the order of  $10^{-11}$  S m $^{-1}$ ,<sup>[42,47]</sup> (unlike conducting MOFs which were also used as active layer in transistors<sup>[48,49]</sup>). After deposition, the HKUST-1 pores were filled with a popular IL of type 1-butyl-3-methylimidazoliumbis(trifluoromethylsulfonyl)imid, referred to as [BMIM][TFSI].<sup>[50]</sup> As previously reported, the Young's modulus of HKUST-1 amounts to  $\approx 10$  GPa<sup>[51]</sup> and the mechanical stability and the Young's modulus even slightly increase when a HKUST-1 MOF is loaded with [BMIM][TFSI].<sup>[52]</sup> On the contrary, adding ionic liquid in polymers to form ion-gels decreases the Young's modulus of the polymer.<sup>[53]</sup> Thus, transferring these properties to the [BMIM][TFSI]@ HKUST-1 film on the GFET suggests that the present material is substantially harder than common ion-gels and possesses a Young's modulus that is  $\approx 2$  orders of magnitude larger.<sup>[51–53]</sup> A top-gated IL@SURMOF/GFET-device was prepared. A thorough analysis of the device's performance revealed high charge densities and mobilities. Compared to the bottom-gated or IL-free device, the voltage of the Dirac point was found to be much lower, allowing the device operation with small voltages below 1.5 V. Moreover, the sensor performance of the top-gated IL@SURMOF/GFET-device was demonstrated and the shift of the Dirac point under the exposure to water vapor was found to be substantially larger than for other analytes like carbon dioxide and different hydrocarbons. This study introduces the polycyclic-aromatic-hydrocarbon-functionalization of graphene as a substrate for MOF films. We demonstrate for the first time that such MOF films on functionalized graphene can be used in GFETs and when the MOF pores are filled with an electrolyte like IL, it can be used as an ion-gated GFET sensor.

## 2. Results and Discussion

The fabrication of the IL@SURMOF/GFET device is schematically depicted in Figure 1. First, the graphene (Graphenea, Spain) was functionalized by immersion into a solution of 1-pyrenemethanol (Pyr-CH<sub>2</sub>OH) in acetonitrile, following standard protocols.<sup>[44]</sup> Then, an HKUST-1 SURMOF was deposited in a layer-by-layer (LBL) fashion, see Figure S1 (Supporting Information). Subsequently, the SURMOF pores were loaded with IL of type [BMIM][TFSI] by immersion into pure IL. Finally, a top gate electrode was added by depositing a small soft indium metal globulite on the IL@SURMOF surface. The contact area was  $\approx 1$  mm<sup>2</sup>.

Raman spectroscopy was used for the characterization of the samples, **Figure 2a**. The Raman data not only show the presence of graphene but also allow to identify structural and chemical modifications.<sup>[54]</sup> The characteristic graphene G- and 2D-Raman peaks in the spectrum of the pristine graphene were observed at 1596 and 2690 cm $^{-1}$ , respectively.<sup>[55]</sup> The Pyr-CH<sub>2</sub>OH functionalized graphene possesses G- and 2D-Raman peaks at 1586 and 2683 cm $^{-1}$ , respectively. Compared to the pristine graphene,

after the deposition of HKUST-1 SURMOF on the functionalized graphene, the G- and 2D-bands were found to be shifted to 1597 and 2692 cm $^{-1}$ , respectively. The G- and 2D-peaks of the IL-loaded SURMOF are at 1597 and 2689 cm $^{-1}$ , i.e., slightly red-shifted compared to the empty SURMOF-graphene sample. After adsorption of the pyrene, the intensity of the defect-related graphene D-band at  $\approx 1350$  cm $^{-1}$  increased but was still relatively small, indicating a very small defect density.<sup>[56]</sup> Upon SURMOF growth and IL-loading, the intensity of the D-band did not increase further. The 2D/G band intensity ratio in all four spectra was found to be larger than one, which also reveals that the amount of additional defects introduced in the graphene by the SURMOF deposition is small and that the quality of the graphene layer remained very high.<sup>[57]</sup> The two-phonon combination mode in graphene, i.e., G\* or D+D' peak, can be observed in all four spectra at  $\approx 2460$  cm $^{-1}$ .<sup>[58]</sup> After the SURMOF deposition and the IL loading, the spectrum of the IL@SURMOF contains all the peaks of the HKUST-1 SURMOF and graphene and additional Raman bands were observed, see Figure 2b. The peaks at 745 and 828 cm $^{-1}$  belong to C-H out-of-plane bending modes of the benzene rings present in the MOF linker molecule, whereas the band at 1007 cm $^{-1}$  stems from the C=C vibration.<sup>[45,59]</sup> The peak at 1460 cm $^{-1}$  corresponds to the symmetric stretching O–C–O vibration of the MOF linkers.<sup>[59]</sup> The peak at 1237 cm $^{-1}$  is assigned to the SO<sub>2</sub> asymmetric stretch vibration in the TFSI anion.<sup>[60]</sup> The Raman peaks at 2871 and 2964 cm $^{-1}$ , as shown in the zoom-in of Figure 2b, provide solid evidence for the existence of the BMIM cation.<sup>[60]</sup> These Raman peaks are considered as the finger prints of the cation and belong to the C–H stretching mode. The Raman peaks of SiO<sub>2</sub>/Si substrate are also evident in the region 946 and 986 cm $^{-1}$ .<sup>[61,62]</sup> The most intense peak at 520 cm $^{-1}$ , which belongs to SiO<sub>2</sub>/Si can be seen in supporting information, Figure S3 (Supporting Information).

The X-ray diffractogram (XRD) displayed in Figure 2c reveals that the film grown on the Pyr-CH<sub>2</sub>OH-functionalized graphene possesses the targeted HKUST-1 structure, with a preferential orientation of the (111) direction perpendicular to the substrate, similar to the case of HKUST-1 SURMOFs grown on other hydroxyl-terminated organic surfaces.<sup>[25,63]</sup> Upon IL loading, no changes of XRD peak positions were observed. However, a substantial variation of the relative peak intensities was observed. Such changes in form factor are expected, since the loading with the IL leads to a strong change of the electron density relative to the empty SURMOF. For example, the intensity ratios of the (200) reflex versus (400) are 1.56 and 0.47 for the pristine SURMOF and the IL-loaded SURMOF, respectively. This is line with the calculated XRDs of HKUST-1 and IL@HKUST-1, Figure S10 (Supporting Information), where the intensity ratio of (200)/(400) reflexes also decreases significantly. This is a clear indication of the embedment of X-ray scatters (here IL) in the MOF pores. The stability of the material during the course of the experiments was also verified by the X-ray diffractograms, which show no change, see Figure S15 (Supporting Information), indicating high stability.

Scanning electron microscopy (SEM) images (Figure 2d) revealed that the HKUST-1 SURMOF deposition on the functionalized graphene yielded a continuous, homogenous thin film with a thickness of  $\approx 300$  nm. This means the dielectric layer is much thinner than the dielectric layers in most other ion-gated GFETs

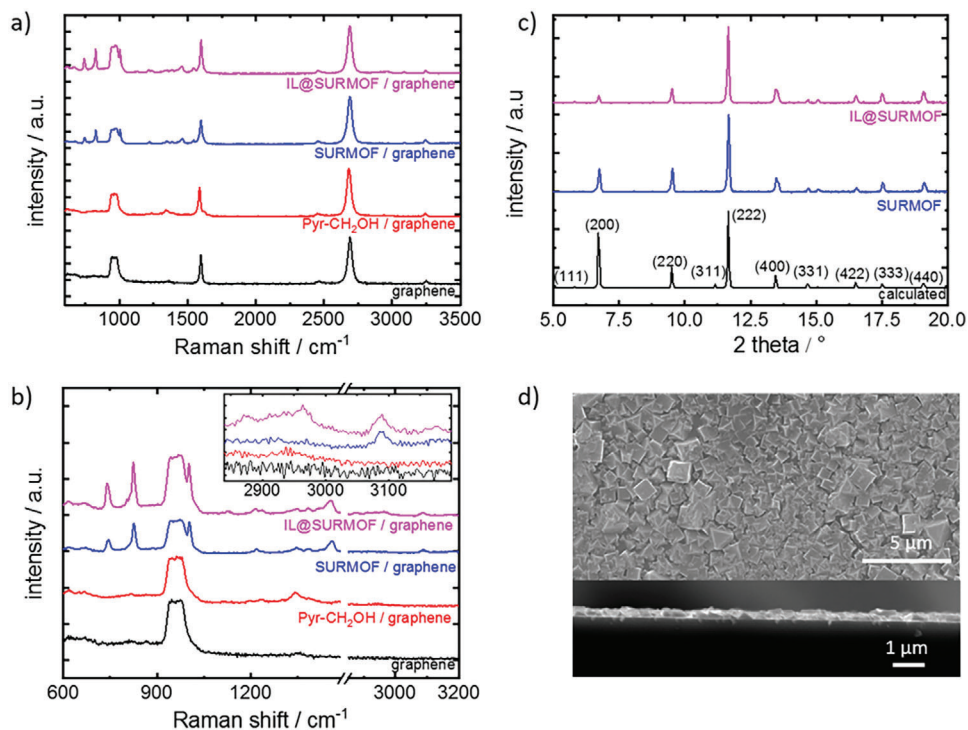


**Figure 2.** a) and b) Raman spectra of graphene (black), Pyr- $\text{CH}_2\text{OH}$ /graphene (red), SURMOF/graphene (blue) and IL@SURMOF/graphene (magenta). The substrate below the graphene monolayer is  $\text{SiO}_2/\text{Si}$ -wafer. (Please note: The data in a) and b) are identical. The strong graphene bands are not shown in b), focusing on the MOF and IL bands.) c) Out-of-plane X-ray diffractogram (XRD) of the HKUST-1 SURMOF grown on Pyr- $\text{CH}_2\text{OH}$  functionalized graphene (blue), of the IL-loaded sample (violet) and the calculated diffractogram of HKUST-1 (black). The diffraction peaks are labelled. d) SEM images of the SURMOF/graphene sample. Above: top view and below: the cross-section of the broken sample. The scale bars are given in the pictures.

where ionic materials of several tens of  $\mu\text{m}$  thickness and more are used.<sup>[34,64]</sup>

The samples were further characterized by atomic force microscopy (Figure S13, Supporting Information) and Energy-dispersive X-ray spectroscopy (EDX) and mapping (Figure S14, Supporting Information), also indicating a homogenous film morphology with a homogenous distribution of elements.

In reference experiments, we used nonfunctionalized (plain) graphene as substrate for the SURMOF synthesis. There, the same procedure did not result in crystalline MOF films, see Figure S2 (Supporting Information). Most of the graphene substrate remains blank and no deposited MOF material was found. Only some small regions with some deposited material were found, see Figure S2 (supporting information). The XRD also shows no reflexes of HKUST-1.

The transistor performance of the IL@SURMOF/GFET device was characterized in an inert nitrogen atmosphere. The transfer curves, **Figure 3a**, of the device were measured by applying a 10 mV bias voltage between the drain and source electrodes ( $V_{\text{DS}}$ ). The voltage between the gate and source electrodes ( $V_{\text{GS}}$ ) was varied between  $-30$  and  $+70$  V in an up-down cycle. The devices with an empty SURMOF showed a poor performance, there was no clear Dirac point (i.e., conductance minimum) in the range below 70 V gate voltage. Such devices are also reported in the literature where high p-type doping of the graphene results in a large Dirac point voltage.<sup>[20]</sup> The hysteresis observed in the transfer curve in **Figure 3a** is a typical behavior for GFETs.<sup>[65]</sup> Af-

ter IL-loading, the transfer curves change tremendously, with a Dirac point at  $V_{\text{Dirac}}$  equal to  $+26.5$  and  $+32.80$  V for the up and down voltage cycle, respectively, see **Figure S4** (Supporting Information). A further substantial improvement occurred when going from the bottom-gate to the top-gate setup (see **Figure S12**, Supporting Information), now the Dirac point was observed at  $-0.159$  and  $-0.299$  V, respectively, see **Figure 3a**. The On-Off ratio of the top-gated IL@SURMOF/GFET device amounted to 13, which is comparable with the On-Off ratio of other ion-gated GFETs.<sup>[28]</sup> Further, the output curves of the IL@SURMOF/GFET device were also recorded at different gate voltages, see **Figure S11** (Supporting Information). The leakage current ( $I_{\text{GS}}$ ) is about three orders of magnitude smaller than the drain-source current ( $I_{\text{DS}}$ ) showing the absence of shortcuts, see **Figure S24** (Supporting Information).

The device performance was further characterized using impedance spectroscopy. The capacitance of the channel versus gate electrode was found to be  $6.8 \mu\text{F cm}^{-2}$  at 1 Hz, see **Figure S6** (Supporting Information). The charge carrier density calculated from this capacitance amounts to  $25 \times 10^{-12} \text{ cm}^{-2}$  see **Figure S7** (Supporting Information). The charge carrier mobility was calculated to be  $385 \text{ cm}^2 \text{ V}^{-1} \text{ s}^{-1}$  for the electrons and  $488 \text{ cm}^2 \text{ V}^{-1} \text{ s}^{-1}$  for the holes, see **Figure S7** (Supporting Information). The charge carrier density and mobilities are comparable with other GFETs,<sup>[29,66]</sup> indicating that the excellent electronic transport properties of graphene are not affected by the SURMOF deposition and IL-loading. Reference experiments with plain

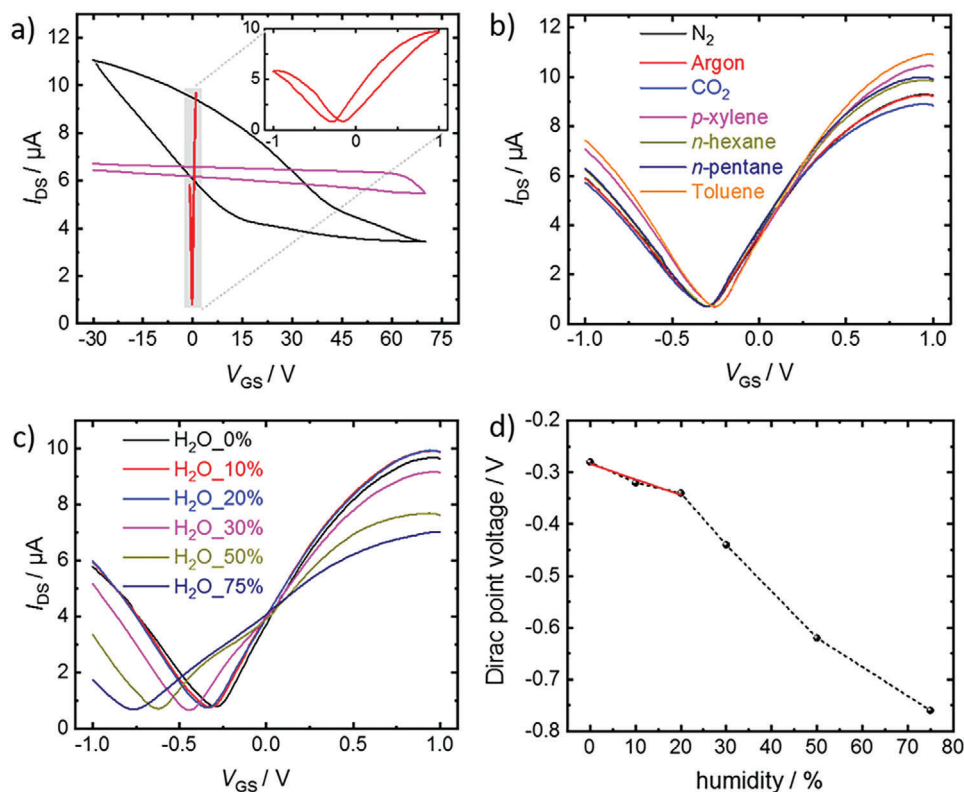


**Figure 3.** a) Transfer curves (i.e.,  $I_{DS}-V_{GS}$ ) of the IL@SURMOF/GFET with a top-gate (red) and its zoom-in as well as of the SURMOF/GFET with a bottom-gate (black) and a top-gate (magenta, without IL). The atmosphere is pure nitrogen. b) Transfer curves (i.e.,  $I_{DS}-V_{GS}$ ) of IL@SURMOF/GFET with a top-gate. The device is exposed to various gases and vapors. Nitrogen (black), argon (red) and  $\text{CO}_2$  (blue) are pure gases. *p*-xylene (magenta), *n*-hexane (dark yellow), *n*-pentane (navy), and toluene (orange) are (pure) vapors in nitrogen. Only the down-voltage-part of the transfer curve is shown for sake of clarity. c) Transfer curves of the same device with various concentrations of water vapor (i.e., various relative humidities), see labels. d) Absolute Dirac point voltages corresponding to various humidity levels. The slope of the red line is the sensitivity of the device at low water concentrations.

(liquid) IL of type [BMIM][TFSI] on the GFET device without a MOF film were performed, see Figure S9 (Supporting Information). The transfer curve and the Dirac point (+0.17 V and +0.06 V, respectively) are similar to the IL@SURMOF/GFET device. However, the liquid nature of the IL hinders the device application.

In the next step, we explored the sensor performance of the IL@SURMOF/GFET device. To this end, the change of the transfer curves and Dirac points in response to the exposure to different analytes in the surrounding atmosphere was investigated, Figure 3b. The following analytes were used: *p*-xylene, *n*-hexane, *n*-pentane, and toluene (as typical volatile organic compounds), carbon dioxide, argon, and water. Among these analytes, especially carbon dioxide and water are well known for the high affinities towards ionic liquids.<sup>[67]</sup> For sake of clarity, we focus on the down-voltage-cycle. In a pure nitrogen atmosphere, the device possesses a Dirac point with a voltage of  $-0.299$  V. For the exposure to Ar,  $\text{CO}_2$ , *n*-hexane, and *n*-pentane, the voltage of the Dirac points does not show a visible shift. Exposed to xylene and toluene vapors, the Dirac point shifts slightly positive to  $-0.258$  V for xylene and to  $-0.259$  V for toluene, respectively. This means, in the saturate vapor pressure of these two analytes, the Dirac points shift by +41 and +40 mV, respectively. When exposed to water vapor, the Dirac point shows a pronounced monotonic shift

to negative gate voltages. During the exposure to 10% and 20% relative humidity, the values of the Dirac voltage shift by  $-20$  and  $-40$  mV, respectively. ( $-0.32$  V for 10% humidity and  $-0.34$  V for 20% humidity.) By further increasing the humidity levels, the observed values for  $V_{\text{Dirac}}$  are:  $-0.44$  V for 30% humidity,  $-0.62$  V for 50% humidity and  $-0.76$  V for 75% humidity, see Figure 3d and Figure S18 (Supporting Information). This observation indicates that a large number of water molecules adsorbed at the IL@SURMOF-graphene interface. Although, water is generally considered as p-type dopant to graphene,<sup>[68]</sup> the results of our device show that graphene has become *n*-doped after exposing the device to water. We suppose that the doping is caused by the rather complex interaction of the ionic liquid at the graphene interface, which is affected by the presence of water.<sup>[69,70]</sup>

Repeating the transfer curve measurements results in the same outcome, see Figures S16 and S17 (Supporting Information). Before measuring the transfer curve for each analyte, the transfer curve in an  $\text{N}_2$  atmosphere was recorded. The  $V_{\text{Dirac}}$  value of all intermediate  $\text{N}_2$  atmosphere were essentially the same, see Figure S18 (Supporting Information). This indicates an excellent reversibility of the device.

The limit of detection (LOD) for water is calculated by  $3 \times$  the standard deviation divided by the sensitivity.<sup>[71]</sup> The sensitivity is the slope of line  $V_{\text{Dirac}}/\%_{\text{humidity}}$  (see Figure 3d) and the standard

deviation is determined from the baseline in pure nitrogen. There, the standard deviation of the Dirac point is 10 mV. The obtained LOD for water is  $0.9\%_{\text{humidity}}$ .

For reference, another device was prepared and explored for analyte sensing. A similar device performance was found with a significant shift of  $V_{\text{Dirac}}$  for  $\text{H}_2\text{O}$  ( $-380$  mV for saturated water vapor) and essentially no change of  $V_{\text{Dirac}}$  for  $\text{N}_2$ , xylene and  $\text{CO}_2$ , see Figure S19 (Supporting Information). In addition, the transfer curves of several tested devices of pristine GFETs, i.e., the used substrates (with bottom-gate electrode), and of the IL@SURMOF/GFETs (with top-gate electrode) are shown for comparison in Figures S22 and S23 (Supporting Information). For different devices of the same type, the curves show only a small variation with slightly different Dirac points.

Comparing the transfer curves of the pristine GFET (Figure S5, Supporting Information) and of the IL@SURMOF/GFET (Figure S19, Supporting Information) shows that the conduction and on-off ratio decrease somewhat (roughly by a factor 2) by the functionalization of the graphene with the IL@SURMOF film. However, more important than the small decrease in channel conductance is the gained significant enhancement in functionality, including ion-gating and working at low voltage as well as making a sensor with a high selectivity and sensitivity.

### 3. Conclusion

A solid-state ion-gated GFET is presented based on nanoporous MOF films with embedded ionic liquid in the pores grown on graphene, which is functionalized with a polycyclic aromatic hydrocarbon, here 1-pyrenemethanol. The SURMOF films were grown in a layer-by-layer fashion, yielding monolithic, crystalline, and highly oriented thin films of homogeneous thickness. The high quality of the IL@SURMOF on the graphene substrate was evidenced by X-ray diffraction, scanning electron microscopy, and Raman spectroscopy. The top-gated IL@SURMOF/GFET device showed excellent device performance with a clear Dirac point, an On-Off ratio of  $\approx 13$ , charge densities above  $10^{-11} \text{ cm}^{-2}$ , as well as electron and hole mobilities of  $\approx 500 \text{ cm}^2 \text{ V}^{-1} \text{ s}^{-1}$ . Due to the porous nature of the SURMOF, the IL@SURMOF/GFET device showed a pronounced response to the gas atmosphere surrounding the device. While the Dirac points showed no shifts or only small positive shifts for analytes like carbon dioxide, argon, xylene, *n*-hexane, *n*-pentane, or toluene, the voltage of the Dirac point decreases substantially when exposed to water.

Our results demonstrate that IL@SURMOF/GFET devices carry a huge potential for sensing applications. This novel device combines the advantages of both material classes: the outstanding electronic properties of the 2D material graphene on the one hand, and the wide tunability of MOFs as well as their excellent selectivity in sensing applications on the other hand. The introduced method to use polycyclic aromatic hydrocarbon to functionalize the 2D material enables a controlled approach to prepare such hybrid devices.

### 4. Experimental Section

*Functionalization of Graphene, SURMOF Synthesis, and IL Loading:* The GFET substrates were purchased from Graphenea, Spain. The source

and drain electrodes are made of gold. The graphene was deposited on  $\text{Si}/\text{SiO}_2$  substrates. The thicknesses of  $\text{SiO}_2$  and Si are 90 nm and 525  $\mu\text{m}$ , respectively. The size of the graphene channel amounted to  $20 \mu\text{m} \times 20 \mu\text{m}$ .

The GFETs were functionalized by immersion in a 3.6 mM 1-pyrenemethanol solution in acetonitrile (ACN), following literature directions.<sup>[44]</sup> The substrates were immersed in the solution for 1 h and rinsed three times with ACN and dried in an  $\text{N}_2$  stream. The SURMOF films on the functionalized substrates were prepared with the LBL method, previously discussed in detail.<sup>[72]</sup> In the LBL synthesis, substrates were alternatively exposed to ethanolic metal-node (here: 1 mM Cu-acetate) and linker (here: 0.2 mM BTC, i.e., benzene-1,3,5-tricarboxylic acid) solutions and the samples were cleaned with pure ethanol between each exposure step. The SURMOFs on the substrates were grown by using a spray method<sup>[73]</sup> with 50 LBL synthesis cycles. The SURMOF samples were loaded with IL by immersion in pure IL for 30 min.<sup>[42]</sup> Before performing the electrical characterization, the excess ionic liquid was removed in a strong  $\text{N}_2$  stream.

Cu-acetate (>98%) and BTC (>98%) were purchased from Alpha Aesar, IL (99.9%) from proionic (proionic.com).

XRDs were recorded in out-of-plane geometry using a Bruker D8 advanced diffractometer equipped with a position sensitive detector in  $\theta$ - $2\theta$  geometry. X-ray radiation with a wavelength of 0.154 nm was used.

All Raman spectroscopy measurements were carried out on the samples made on 90-nm  $\text{SiO}_2/\text{Si}$  substrate under ambient conditions using a Bruker Senterra Raman microscope. A laser of 532 nm wavelength with 2.5 mW power was used. Raman spectra of graphene and pyrenemethanol functionalized graphene were recorded at 50X magnification and the spot size was  $\approx 5 \mu\text{m}^2$ . The SURMOF and IL loaded SURMOF samples were measured at 20X magnification and a spot size of  $\approx 80 \mu\text{m}^2$ . The data acquisition and spectra analysis were performed using Bruker OPUS software 7.8. For all samples, the Raman spectra were recorded at three different positions and their intensities were added. The spectra were normalized with respect to the 2D peak of graphene.

*Electrical Transport Measurements:* The transport properties of the fabricated GFET device were measured using two Keithley source meter units (SMUs), 2635B and 2450. For the measurements, the voltage between source and drain electrode was applied using SMU 2536B and the current was recorded. The gate bias was applied using SMU 2450 and the current was recorded, verifying no leakage current.

For the electrical measurements, the sample was placed in a home-built chamber. The gas atmosphere is controlled by purging the chamber with nitrogen that can be enriched with different gas or vapor molecules. *p*-xylene, *n*-hexane, *n*-pentane, toluene, and water vapors were realized by the nitrogen flow passing through the wash bottle (i.e., bubbler) filled with the respective liquids. In this way, vapor pressures close to the saturated vapor pressure are realized.<sup>[74,75]</sup> The saturated vapor pressure are: *p*-xylene (13.1 mbar), *n*-hexane (204.9 mbar), *n*-pentane (670 mbar), toluene (28.8 mbar) and water (31.6 mbar). Water vapor with reduced concentration (10% relative humidity, 20% etc.) was prepared by mixing a pure nitrogen flow and a nitrogen flow enriched with the water vapor in different ratios.<sup>[76]</sup> Pure  $\text{CO}_2$ ,  $\text{N}_2$ , and Ar gases were purged in the chamber for creating a pure gas atmosphere (with a pressure of 1 atm). All the measurements were carried out at room temperature ( $\approx 295$  K). Before the measurements, the sample was equilibrated for 20 min in the new analyte atmosphere, which is sufficient time for the analyte molecules to diffuse to the graphene-IL@SURMOF interface.

### Supporting Information

Supporting Information is available from the Wiley Online Library or from the author.

### Acknowledgements

The authors are thankful to Ralph Krupke (KIT) for his comments and fruitful discussions. The authors also acknowledge funding by the German

Research Foundation (DFG HE 7036/5 and SPP-1928 COORNETs), by the Virtual Materials Design (VirtMat) initiative at KIT and by the European Union. Funded by the European Union (ERC, DYONCON, 101043676). Views and opinions expressed are however those of the author(s) only and do not necessarily reflect those of the European Union or the European Research Council. Neither the European Union nor the granting authority can be held responsible for them.

Open access funding enabled and organized by Projekt DEAL.

## Conflict of Interest

The authors declare no conflict of interest.

## Author Contributions

The manuscript was written through contributions of all authors. All authors have given approval to the final version of the manuscript.

## Data Availability Statement

The data that support the findings of this study are available from the corresponding author upon reasonable request. The data are also available on Radar4Chem (<https://www.radar-service.eu>), DOI: 10.22000/1105.

## Keywords

graphene field-effect transistors, ion-gated transistors, ionic liquids, metal-organic framework thin films, sensors

Received: October 13, 2022

Revised: May 24, 2023

Published online:

- [1] A. K. Geim, I. V. Grigorieva, *Nature* **2013**, 499, 419.
- [2] A. K. Geim, *Science* **2009**, 324, 1530.
- [3] Y. Wang, L. Wang, T. Yang, X. Li, X. Zang, M. Zhu, K. Wang, D. Wu, H. Zhu, *Adv. Funct. Mater.* **2014**, 24, 4666.
- [4] G. Y. Bae, S. W. Pak, D. Kim, G. Lee, D. H. Kim, Y. Chung, K. Cho, *Adv. Mater.* **2016**, 28, 5300.
- [5] C. Soldano, A. Mahmood, E. Dujardin, *Carbon* **2010**, 48, 2127.
- [6] K. Novoselov, o. A. Mishchenko, o. A. Carvalho, A. Castro Neto, *Science* **2016**, 353, aac9439.
- [7] L. Lin, B. Deng, J. Sun, H. Peng, Z. Liu, *Chem. Rev.* **2018**, 118, 9281.
- [8] A. Nag, A. Mitra, S. C. Mukhopadhyay, *Sens. Actuators, A* **2018**, 270, 177.
- [9] O. Moldovan, B. Iñiguez, M. J. Deen, L. F. Marsal, *IET Circuits, Devices & Systems* **2015**, 9, 446.
- [10] S. Wu, Q. He, C. Tan, Y. Wang, H. Zhang, *Small* **2013**, 9, 1160.
- [11] B. Davaji, H. D. Cho, M. Malakoutian, J.-K. Lee, G. Panin, T. W. Kang, C. H. Lee, *Sci. Rep.* **2017**, 7, 8811.
- [12] K. Xia, C. Wang, M. Jian, Q. Wang, Y. Zhang, *Nano Res.* **2018**, 11, 1124.
- [13] A. Farmani, A. Mir, *IEEE Photonics Technol. Lett.* **2019**, 31, 643.
- [14] H. Kishikawa, M. Sato, N. Goto, S.-i. Yanagiya, T. Kaito, S.-K. Liaw, *Jpn. J. Appl. Phys.* **2019**, 58, SJJD05.
- [15] A. Ahmed, I. Hassan, I. M. Mosa, E. Elsanadidy, M. Sharafeldin, J. F. Rusling, S. Ren, *Adv. Mater.* **2019**, 31, 1807201.
- [16] M. Magliulo, A. Mallardi, R. Cristina, F. Ridi, L. Sabbatini, N. Cioffi, G. Palazzo, L. Torsi, *Anal. Chem.* **2013**, 85, 3849.
- [17] D. Zhan, J. Yan, L. Lai, Z. Ni, L. Liu, Z. Shen, *Adv. Mater.* **2012**, 24, 4055.
- [18] N. Chauhan, T. Maekawa, D. N. S. Kumar, *J. Mater. Res.* **2017**, 32, 2860.
- [19] X. Yu, H. Cheng, M. Zhang, Y. Zhao, L. Qu, G. Shi, *Nat. Rev. Mater.* **2017**, 2, 17046.
- [20] S. Kumar, Y. Pramudya, K. Müller, A. Chandresh, S. Dehm, S. Heidrich, A. Fediai, D. Parmar, D. Perera, M. Rommel, L. Heinke, W. Wenzel, C. Wöll, R. Krupke, *Adv. Mater.* **2021**, 33, 2103316.
- [21] H. Furukawa, K. E. Cordova, M. O'Keeffe, O. M. Yaghi, *Science* **2013**, 341, 1230444.
- [22] A. Chidambaram, K. C. Stylianou, *Inorg. Chem. Front.* **2018**, 5, 979.
- [23] P. Qin, B. A. Day, S. Okur, C. Li, A. Chandresh, C. E. Wilmer, L. Heinke, *ACS Sens.* **2022**, 7, 1666.
- [24] M. Woellner, S. Hausdorf, N. Klein, P. Mueller, M. W. Smith, S. Kaskel, *Adv. Mater.* **2018**, 30, 1704679.
- [25] O. Shekhah, H. Wang, S. Kowarik, F. Schreiber, M. Paulus, M. Tolan, C. Sternemann, F. Evers, D. Zacher, R. A. Fischer, *J. Am. Chem. Soc.* **2007**, 129, 15118.
- [26] L. Heinke, C. Wöll, *Adv. Mater.* **2019**, 31, 1806324.
- [27] Y. Ohno, K. Maehashi, Y. Yamashiro, K. Matsumoto, *Nano Lett.* **2009**, 9, 3318.
- [28] A. Das, S. Pisana, B. Chakraborty, S. Piscanec, S. K. Saha, U. V. Waghmare, K. S. Novoselov, H. R. Krishnamurthy, A. K. Geim, A. C. Ferrari, *Nat. Nanotechnol.* **2008**, 3, 210.
- [29] B. J. Kim, H. Jang, S.-K. Lee, B. H. Hong, J.-H. Ahn, J. H. Cho, *Nano Lett.* **2010**, 10, 3464.
- [30] R. D. Rogers, K. R. Seddon, *Science* **2003**, 302, 792.
- [31] A. Inaba, K. Yoo, Y. Takei, K. Matsumoto, I. Shimoyama, *Sens. Actuators, B* **2014**, 195, 15.
- [32] A. Janissek, J. Lenz, F. d. Giudice, M. Gaulke, F. Pyatkov, S. Dehm, F. Hennrich, L. Wei, Y. Chen, A. Fediai, M. Kappes, W. Wenzel, R. Krupke, R. T. Weitz, *App. Phys. Lett.* **2021**, 118, 063101.
- [33] J. H. Cho, J. Lee, Y. Xia, B. Kim, Y. He, M. J. Renn, T. P. Lodge, C. Daniel Frisbie, *Nat. Mater.* **2008**, 7, 900.
- [34] D. S. Liu, U. Khan, P. Li, M. A. Khan, J. Wu, Z. Wang, *IEEE Sens. J.* **2021**, 21, 18483.
- [35] H. Chun, T. D. Chung, *Annu. Rev. Anal. Chem.* **2015**, 8, 441.
- [36] S. Z. Bisri, S. Shimizu, M. Nakano, Y. Iwasa, *Adv. Mater.* **2017**, 29, 1607054.
- [37] S. Y. Yang, F. Cicoira, R. Byrne, F. Benito-Lopez, D. Diamond, R. M. Owens, G. G. Malliaras, *Chem. Commun.* **2010**, 46, 7972.
- [38] K. Kim, C. L. Chen, Q. Truong, A. M. Shen, Y. Chen, *Adv. Mater.* **2013**, 25, 1693.
- [39] K. Fujie, H. Kitagawa, *Coord. Chem. Rev.* **2016**, 307, 382.
- [40] K. Fujie, K. Otsubo, R. Ikeda, T. Yamada, H. Kitagawa, *Chem. Sci.* **2015**, 6, 4306.
- [41] Z. Zhang, M. Liu, C. Li, W. Wenzel, L. Heinke, *Small* **2022**, 18, 2200602.
- [42] A. B. Kanj, R. Verma, M. Liu, J. Helfferich, W. Wenzel, L. Heinke, *Nano Lett.* **2019**, 19, 2114.
- [43] X. V. Zhen, E. G. Swanson, J. T. Nelson, Y. Zhang, Q. Su, S. J. Koester, P. Bühlmann, *ACS Appl. Nano Mater.* **2018**, 1, 2718.
- [44] X. V. Zhen, E. G. Swanson, J. T. Nelson, Y. Zhang, Q. Su, S. J. Koester, P. Bühlmann, *ACS Appl. Nano Mater.* **2018**, 1, 2718.
- [45] C. Prestipino, L. Regli, J. G. Vitillo, F. Bonino, A. Damin, C. Lamberti, A. Zecchina, P. Solari, K. Kongshaug, S. Bordiga, *Chem. Mater.* **2006**, 18, 1337.
- [46] K. Müller, K. Fink, L. Schöttner, M. Koenig, L. Heinke, C. Wöll, *ACS Appl. Mater. Interfaces* **2017**, 9, 37463.
- [47] J. Liu, T. Wächter, A. Irmiler, P. G. Weidler, H. Gliemann, F. Pauly, V. Mugnaini, M. Zharnikov, C. Wöll, *ACS App. Mat. Int.* **2015**, 7, 9824.

- [48] G. D. Wu, J. H. Huang, Y. Zang, J. He, G. Xu, *J. Am. Chem. Soc.* **2017**, *139*, 1360.
- [49] B. Wang, Y. Luo, B. Liu, G. Duan, *ACS App. Mat. Int.* **2019**, *11*, 35935.
- [50] A. Dragässer, O. Shekhah, O. Zybalyo, C. Shen, M. Buck, C. Wöll, D. Schlettwein, *Chem. Commun.* **2012**, *48*, 663.
- [51] S. Bundschuh, O. Kraft, H. Arslan, H. Gliemann, P. Weidler, C. Wöll, *Appl. Phys. Lett.* **2012**, *101*, 101910.
- [52] S.-G. Koh, T. Koide, A. Arai, I. Ohira, K. Kinoshita, *J. Phys. Chem. C* **2022**, *126*, 6736.
- [53] J. C. Jansen, K. Friess, G. Clarizia, J. Schauer, P. Izak, *Macromolecules* **2011**, *44*, 39.
- [54] A. C. Ferrari, D. M. Basko, *Nat. Nanotechnol.* **2013**, *8*, 235.
- [55] A. Das, B. Chakraborty, A. Sood, *Bull. Mater. Sci.* **2008**, *31*, 579.
- [56] C. Xie, P. Lv, B. Nie, J. Jie, X. Zhang, Z. Wang, P. Jiang, Z. Hu, L. Luo, Z. Zhu, *Appl. Phys. Lett.* **2011**, *99*, 133113.
- [57] X. Li, W. Cai, J. An, S. Kim, J. Nah, D. Yang, R. Piner, A. Velamakanni, I. Jung, E. Tutuc, *Science* **2009**, *324*, 1312.
- [58] P. May, M. Lazzeri, P. Venezuela, F. Herziger, G. Callsen, J. S. Reparaz, A. Hoffmann, F. Mauri, J. Maultzsch, *Phys. Rev. B* **2013**, *87*, 075402.
- [59] M. Todaro, A. Alessi, L. Sciortino, S. Agnello, M. Cannas, F. M. Gelardi, G. Buscarino, *J. Spectrosc.* **2016**, *2016*, 8074297.
- [60] J. Wu, X. Zhu, H. Li, L. Su, K. Yang, X. Cheng, G. Yang, J. Liu, *J. Solution Chem.* **2015**, *44*, 2106.
- [61] V. Mankad, S. K. Gupta, P. K. Jha, N. Ovsyuk, G. Kachurin, *J. Appl. Phys.* **2012**, *112*, 054318.
- [62] P. Spizzirri, J.-H. Fang, S. Rubanov, E. Gauja, S. Praver, *arXiv:1002.2692*, **2010**.
- [63] O. Shekhah, H. Wang, D. Zacher, R. A. Fischer, C. Wöll, *Angew. Chem., Int. Ed.* **2009**, *48*, 5038.
- [64] Y.-L. He, J.-B. Liu, T.-L. Wen, Q.-H. Yang, Z. Feng, W. Tan, X.-S. Li, Q.-Y. Wen, H.-W. Zhang, *Mater. Res. Express* **2018**, *5*, 115607.
- [65] H. Wang, Y. Wu, C. Cong, J. Shang, T. Yu, *ACS Nano* **2010**, *4*, 7221.
- [66] S.-K. Lee, B. J. Kim, H. Jang, S. C. Yoon, C. Lee, B. H. Hong, J. A. Rogers, J. H. Cho, J.-H. Ahn, *Nano Lett.* **2011**, *11*, 4642.
- [67] M. Smiglak, J. M. Pringle, X. Lu, L. Han, S. Zhang, H. Gao, D. R. MacFarlane, R. D. Rogers, *Chem. Comm.* **2014**, *50*, 9228.
- [68] F. Schedin, A. K. Geim, S. V. Morozov, E. W. Hill, P. Blake, M. I. Katsnelson, K. S. Novoselov, *Nat. Mater.* **2007**, *6*, 652.
- [69] C. Melios, C. E. Giusca, V. Panchal, O. Kazakova, *2D Mater.* **2018**, *5*, 022001.
- [70] C. Verma, E. E. Ebenso, *Graphene Technology* **2019**, *4*, 1.
- [71] G. L. Long, J. D. Winefordner, *Anal. Chem.* **1983**, *55*, 712A.
- [72] O. Shekhah, J. Liu, R. a. Fischer, C. Wöll, *Chem. Soc. Rev* **2011**, *40*, 1081.
- [73] S. Hurrle, S. Friebe, J. Wohlgemuth, C. Wöll, J. Caro, L. Heinke, Sprayable, *Chem.-Eur. J.* **2017**, *23*, 2294.
- [74] P. Qin, S. Okur, C. Li, A. Chandresh, D. Mutruc, S. Hecht, L. Heinke, *Chem. Sci.* **2021**, *12*, 15700.
- [75] C. Li, Z. Zhang, L. Heinke, *Phys. Chem. Chem. Phys.* **2022**, *24*, 3994.
- [76] P. Qin, S. Okur, Y. Jiang, L. Heinke, *J. Mater. Chem. A* **2022**, *10*, 25347.